MOMENTUM AND HEAT TRANSPORT IN THE WAKE OF TWO TANDEM CYLINDERS

G. Xu and **Y. Zhou**
Department of Mechanical Engineering
The Hong Kong Polytechnic University
Hung Hom, Kowloon, Hong Kong
mmgxu@polyu.edu.hk, mmyzhou@polyu.edu.hk

ABSTRACT

The vortex structures, momentum and heat transport in the wake of two tandem circular cylinders have been investigated. The measurements were conducted at x/d = 10 ~ 30 and Re ($\equiv U_\infty d/\nu$, where d is the cylinder diameter, U_∞ the free stream velocity and ν the kinematic viscosity) = 7000 using a three-wire (an X-wire plus a cold wire) probe, in conjunction with an X-wire. The cylinder center-to-center spacing, L/d, was 1.3, 2.5 and 4, each representing one typical flow regime. The regimes are classified based on whether the shear layers separated from the upstream cylinder form vortices between the cylinders, reattach on or roll up behind the downstream cylinder (without reattachment). The phase-averaged sectional streamlines and vorticity contours display a single vortex street behind the downstream cylinder, irrespective of different flow regimes. However, the flow structure does depend upon L/d in terms of longitudinal and lateral vortex spacing, vortex strength and the downstream decay of vorticity. The momentum and heat transport characteristics of the flow are discussed by examining the coherent and incoherent momentum and heat flux vectors.

1 INTRODUCTION

Modern cities (e.g. New York, Tokyo and Hong Kong) are characterized by many high-rise skyscrapers. It would be crucial for town planners or environmental protection agencies to know or predict how pollutants discharged say by vehicles are dispersed or transported. It is therefore important to understand the transport characteristics of passive scalars behind multiple slender structures. The simplest configuration is one or two cylinders.

The wake of a single cylinder has been extensively investigated in terms of turbulence transport. Matsumura and Antonia (1993) investigated momentum and heat transport in the turbulent intermediate wake of a single circular cylinder at a Reynolds number Re ($\equiv U_\infty d/\nu$, where U_∞, d and ν are the free-stream velocity, cylinder diameter and kinematic viscosity of the fluid, respectively) of 5830. They found that the turbulent Karman vortex street transports heat more effectively than momentum. Also, the net heat transport associated with the vortical motion occurs in the downstream region of each vortex for x/d=10 while at other downstream stations (x/d=20 and 40), the net transport is equally distributed between the upstream and downstream regions of individual vortices.

Investigations, similar to Matsumura and Antonia (1993), behind multiple structures are not many. Zhou et al. (2002) studied the momentum and heat transport in the wake of two side-by-side circular cylinders for x/d=10, 20 and 40 at Re=5800. Their results indicated that the turbulent vortex structures, and the heat and momentum transport depend to a great extent on the transverse spacing T between the two cylinder axes. At T/d=3, the interaction between the vortex streets promotes the transport of heat out of the vortices. At T/d=1.5, the row of vortices of greater strength makes a larger contribution to the Reynolds normal stresses and heat transport than that at T/d=3.

One may surmise that the manner in which momentum and heat transport occurs behind a cylinder in the presence of an upstream cylinder must be different from that behind an isolated cylinder or two side-by-side cylinders. There have been numerous investigations on the flow behind two tandem circular cylinders, most of which focus on the Strouhal numbers, Re effects and forces on the cylinders (e.g. Igarashi, 1981; Zdravkovich, 1987). This flow depends on L/d as well as the Reynolds number, initial conditions and pressure gradient, etc. Zdravkovich (1987) classified the flow around two tandem stationary cylinders into three flow regimes based on the longitudinal spacing L between the cylinder axes. For $1 < L/d < 1.2 \sim 1.8$, the free shear layers separated from the upstream cylinder do not reattach on the downstream cylinder. The vortex street behind the latter is formed by the free shear layers detached from the former. For $1.2 \sim 1.8 < L/d < 3.4 \sim 3.8$, the free shear layers separated from the upstream cylinder reattach on the upstream side of the downstream cylinder. A vortex street is formed only behind the downstream cylinder. For $L/d > 3.4 \sim 3.8$, the separated shear layers roll up alternately and form vortices between each cylinder, both cylinders generating vortices. Igarashi (1981) suggested a similar classification. However, to our knowledge, there has been little information on the momentum and heat transport of this flow in the literature.

This work aims to investigate experimentally how the presence of an upstream cylinder affects the momentum and heat transport in a circular cylinder wake and how the transport differs among the three flow regimes (Zdravkovich 1987). Measurements were made at x/d=10, 20 and 30 for L/d =1.3, 2.5 and 4, each representing a flow regime. The data were

analysed using a phase averaging method developed by Zhou et al. (2002).

2 EXPERIMENTAL CONDITIONS

Experiments were carried out in a close-circuit wind tunnel with a working section of 600 mm × 600 mm, which is 2.4 m long. The wake was generated by two brass circular cylinders of the same diameter d=15 mm, arranged in tandem. U_∞ was 7 m/s, the corresponding Re being about 7000. The downstream cylinder was electrically heated. The maximum mean temperature of the heated wake at x/d = 10 – 30 was about 0.8 ^{0}C above the ambient fluid, implying that the buoyancy effect should be negligible and heat could be considered to be a passive scalar. A three-wire probe consisting of an X-wire and a cold wire was used to measure the longitudinal velocity (u), transverse velocity (v) and temperature (θ) fluctuations. The cold wire was located orthogonally to the plane of the X-wire and about 0.8 mm upstream of the X-wire intersection. An X-wire, placed at y/d = 4 for each measuring station, was also used in conjunction with the three-wire probe so as to provide a phase reference for the signals from the three-wire probe.

The sensing elements of the hot wires were made of 5 μm Pt-10% Rh wire approximately 1 mm in length. For the cold wire, the sensing element was made of 1.27 μm Pt-10% Rh wire about 1.2 mm in length. The temperature coefficient of the cold wire is 1.69×10^{-3} $^0C^{-1}$. The hot wires were operated on constant temperature circuits at an overheat ratio of 1.5. The cold wire was operated on a constant current (0.1 mA) circuit with output proportional to θ. The two probes were calibrated for velocity, yaw angle and temperature in the free stream using a Pitot-static tube connected to a Furness micromanometer and a thermocouple.

Velocity and temperature signals from the anemometer were passed through buck and gain circuits, low-pass filtered and digitised on a personal computer using a 12 bit A/D converter at a sampling frequency $f_{sampling}$ = 3,500 Hz. The sampling duration was 30 s.

3 RESULTS

Figure 1 compares the power spectra, E_u, E_v and E_θ, of u, v and θ at x/d=10 and y/d = 0.5δ for L/d=1.3, 2.5 and 4, where δ is the mean velocity half-width. The u-, v- and θ-spectra all exhibit a pronounced peak at f* = fd/U_∞=0.198 for L/d=1.3 and 2.5, and 0.143 for L/d=4. A minor peak at f*=0.286 is verified to be the second harmonic of the major peak. Hereafter, an asterisk denotes normalization by U_∞, Θ_1 (the maximum temperature difference between the heated flow and the ambient fluid) and d. The observation indicates the occurrence of the dominant vortices in the flow, irrespective the L/d value. Note that the peak in the spectra at L/d=4 is more pronounced than at L/d=1.3 and 2.5, suggesting an increased vortex strength at L/d=4.

A phase averaging method, which is the same as that used by Zhou et al. (2002), was employed to analyze the velocity and temperature signals. Figure 2 presents the iso-contours of the coherent (phased-averaged) spanwise vorticity $\tilde{\omega} = \partial(\overline{V} + \tilde{v})/\partial x - \partial(\overline{U} + \tilde{u})/\partial y$, where $\partial/\partial x = -U_c^{-1}\partial/\partial t$ and U_c is the average convection velocity of vortices, which is identified with the velocity at the maximum $\tilde{\omega}$. A single vortex street only occurs in all cases. The normalized vorticity level associated with vortices at L/d=4 is considerably higher than at L/d= 1.3 and 2.5, which is internally consistent with the more pronounced peak at L/d=4 in spectra (Fig 1). Note that vortex shedding from the upstream cylinder occurs at L/d=4, not at L/d = 1.3 and 2.5. The observation suggests that vortex shedding from the upstream cylinder enhances the strength of vortices. The vortices decay most rapidly at L/d=1.3 and most slowly at L/d=4. The maximum vorticity at x/d=30 amounts to about 30% of that at x/d=10 for L/d=1.3, but 47.8% for L/d=2.5 and 52.3% for L/d=4. The spatial location of vortices at L/d=4 is significantly different from that at L/d=1.3 and 2.5. The longitudinal spacing or vortex wavelength λ at L/d=4 is larger than that at L/d=1.3 and 2.5, consistent with the lower vortex-shedding frequency at this L/d. The lateral spacing at L/d=4 is larger than at L/d = 1.3 and 2.5.

Contours of the phased-averaged temperature $\overline{T} + \tilde{\theta}$ are presented in Figure 3. There is a close similarity between the $\overline{T} + \tilde{\theta}$ and $\tilde{\omega}$ concentrations and the large $\tilde{\omega}$ contours coincide well with high-level isotherms, indicating an association between heat and the large-scale vortical structures. This association appears considerably enhanced at L/d = 4, probably due to the increased vortex strength at this L/d (Fig 2).

Assuming that the conditionally averaged structure begins at p_1 samples (corresponding to $\phi=-\pi$) before $\phi=0$ and ends at p_2 samples (corresponding to $\phi=\pi$) after $\phi=0$, the structural average, denoted by a double overbar, is defined by

$$\overline{\overline{\tilde{q}\tilde{s}}} = \frac{1}{p_1 + p_2 + 1}\sum_{-p_1}^{p_2}\tilde{q}\tilde{s},$$

where s and q stand for either u, v or θ. The ratio of $\overline{\overline{\tilde{q}\tilde{s}}}$ to $\overline{qs}$ provides a measure of the contribution from coherent structures to the Reynolds stresses, temperature variance and heat fluxes. Noting the dependence of this ratio on y, an averaged contribution, $(\overline{\overline{\tilde{q}\tilde{s}}}/\overline{qs})_m$, across the wake, from the coherent structures is defined by

$$(\overline{\overline{\tilde{q}\tilde{s}}}/\overline{qs})_m = \int_{-Y^*}^{Y^*}\left|\overline{\overline{\tilde{q}\tilde{s}}}\right|dy^* / \int_{-Y^*}^{Y^*}\left|\overline{qs}\right|dy^*,$$

where Y* denotes the position at which $\left|\overline{qs}\right|$ is nearly zero. The values of $(\overline{\overline{\tilde{q}\tilde{s}}}/\overline{qs})_m$ are given in Table 1. The coherent contribution to $\overline{v^2}$ is greater than that to either $\overline{u^2}$ or $\overline{\theta^2}$; the contribution to $\overline{\theta^2}$ is the

smallest. This strong contribution to $\overline{v^2}$, previously reported by Kiya and Matsumura (1985) and Antonia (1991) for a single-cylinder wake, is largely ascribed to the enhancement of $\overline{v^2}$ due to the primarily antisymmetrical arrangement of the counter-rotating vortices of the Karman street. On the other hand, the present detection method of vortical structures focuses on the v signal, the contributions to $\overline{u^2}$ and $\overline{\theta^2}$ are thus likely to be underestimated.

The coherent contributions to $\overline{u^2}$, $\overline{v^2}$ and $\overline{\theta^2}$ are always significantly less than their incoherent counterparts at L/d=1.3 and 2.5. A opposite trend is observed for L/d=4.0, except that to the temperature variance $\overline{\theta^2}$. These contributions to $\overline{u^2}$, $\overline{v^2}$ and $\overline{\theta^2}$ at L/d=4.0 is the largest. Generally, these contributions reduce as x/d increases because of the weakening vortical structures and the growth of small-scale structures. The streamwise decrease of the coherent contributions to $\overline{u^2}$, $\overline{v^2}$ and $\overline{\theta^2}$ slows with increasing L/d, in strong contrast to the case of two side-by-side cylinders of Zhou et al. (2002) who found that the coherent contribution to $\overline{u^2}$, $\overline{v^2}$ and $\overline{\theta^2}$ drops fastest at T/d=3.0, reflecting a different vortical structure between the two flows. For example, one obvious difference is that no binary vortex street is observed for the present case while their measurements uncovered the binary vortex streets at T/d=3.0.

The coherent contributions to $\overline{uv}$, $\overline{u\theta}$ and $\overline{v\theta}$ are smaller at L/d=1.3 and 2.5 than those at L/d=4.0. These contributions decrease more rapidly at L/d=1.3 than at L/d=2.5 and 4.0. At x/d=30, there is practically no contribution from the vortical structures to Reynolds shear stress and heat fluxes at L/d=1.3 and 2.5. However, at L/d=4.0, the coherent contributions are still comparable to their corresponding time-averaged counterparts. This is probably because of an appreciably slow vortex decay at L/d = 4, compared with other two cases (Fig 2). The coherent contribution to $\overline{u\theta}$ and $\overline{v\theta}$ is larger than that to $\overline{uv}$, indicating that vortices transport heat more efficiently than transport momentum. This is in agreement with those of the single cylinder wake of Matsumura and Antonia (1993) and the two side-by-side cylinder wake of Zhou et al. (2002).

Figure 4 compares the coherent heat flux vectors $\tilde{\boldsymbol{q}} \equiv (\tilde{u}\tilde{\theta}, \tilde{v}\tilde{\theta})$ and the incoherent heat flux vectors $\boldsymbol{q}_r \equiv (u_r\theta_r, v_r\theta_r)$, along with the coherent velocity vector $\tilde{\boldsymbol{V}} \equiv (\overline{U} + \tilde{u} - U_c, \tilde{v})$, which may shed light upon heat transport associated with the vortical motion. Irrespective of L/d, the coherent heat flux vector $\tilde{\boldsymbol{q}}$ within vortices is approximately aligned with the velocity vector $\tilde{\boldsymbol{V}}$, suggesting that the coherent motion within vortices does not contribute to any net transport of heat out of vortices. Large-magnitude $\tilde{\boldsymbol{q}}$ covers a wider range of y/d at L/d=4.0 than at L/d=1.3 and 2.5. This is because vortices are moving further away from the centerline at L/d=4 and the induced motion carries warmer fluid to larger y/d. $\tilde{\boldsymbol{q}}$ appears to circulate within the vortex for L/d=4.0, different from that at L/d=2.5. The circulation impairs with increasing x/d, and nearly disappears at x/d=30 (not shown). $\tilde{\boldsymbol{q}}$ in the alleyway between vortices is in a direction opposite to the velocity vector, and that in the two sides of vortices changes sign at the saddle points.

Within the vortices, the incoherent heat flux vector $\boldsymbol{q}_r$ generally points upstream, implying that the incoherent motion may hinder the net transport of heat. $\boldsymbol{q}_r$ out of the vortices changes sign in the location of diverging separatrices, indicating heat transport in both upstream and downstream directions.

4 CONCLUSIONS

The heat and momentum transport behind a circular cylinder in the presence of an upstream cylinder have been measured for L/d = 1.3, 2.5 and 4 using a three-wire probe in conjunction with an X-wire. The data were analysed using a phase-averaging technique. The investigation leads to the following conclusions:

1 One single vortex street occurs behind the downstream cylinder, irrespective of different L/d. No binary vortex street is observed for x/d $\geq$ 10. Nonetheless, the detailed flow structure exhibits a strong dependence on L/d in terms of the longitudinal and lateral vortex spacings, vortex strength and the downstream decay of vorticity. This is particularly evident as L/d increases from 2.5 to 4. It is well known that vortex shedding from the upstream cylinder occurs at L/d = 4, but not at L/d = 2.5 or smaller. This difference in the near-wake vortex formation could be largely responsible for the distinct flow structures between L/d = 4 and 2.5 or 1.3.

2 The location of the maximum $\overline{T} + \tilde{\theta}$ corresponds approximately to that of the maximum concentration of $\tilde{\omega}$. This is more evident for increasing L/d. The coherent heat flux vector $\tilde{q}$ within vortices is approximately aligned with the velocity vector $\tilde{V}$. These indicate that vortices tend to retain heat.

3 The coherent contributions to $\overline{u^2}$, $\overline{v^2}$, $\overline{\theta^2}$, $\overline{uv}$, $\overline{u\theta}$ and $\overline{v\theta}$ at L/d=4.0 are significantly larger and exhibit a slower decay than at L/d=1.3 and 2.5. The observation is linked to the vortices of a greater strength at L/d=4.0 than at L/d=2.5 and 1.3.

4 Vortices contribute more to $\overline{u\theta}$ and $\overline{v\theta}$ than to $\overline{uv}$, transporting heat more efficiently than momentum. This is in agreement with those of the single cylinder wake of Matsumura and Antonia (1993) and the two side-by-side cylinder wake of Zhou et al. (2002).

ACKNOWLEDGMENTS

The authors wish to acknowledge support given to them by the Central Research Grant of The Hong Kong Polytechnic University through Grant G-YW74. Mr M W Yiu's contribution to the experimental data analysis is greatly appreciated.

REFERENCES

Igarashi, T. 1981. Characteristics of the flow around two cylinders arranged in tandem, 1st Report. *Bulletin of the JSME*, **B24**, 323-331.

Matsumura, M. & Antonia, R.A. 1993. Momentum and heat transport in the turbulent intermediate wake of a circular cylinder, *J. Fluid Mech.* **250**, 651-668.

Zdravkovich, M. M. 1987. The effects of interference between circular cylinders in cross flow, *Journal of Fluids and Structures*, **1**, 239-261.

Zhou, Y., Zhang, H. J. & Yiu, M.W. 2002. The turbulent wake of two side-by-side circular cylinders, *J. Fluid Mech.* **458**, 303-332.

Table 1: Averaged contributions from the coherent motion to Reynolds stresses, heat fluxes and temperature variance.

L/d	**1.3**			**2.5**			**4.0**		
x/d	*10*	*20*	*30*	*10*	*20*	*30*	*10*	*20*	*30*
$(\overline{\tilde{u}^2}/\overline{u^2})_m(\%)$	44.5	12.6	5.9	18.2	27.7	13.2	81.1	73.8	61.7
$(\overline{\tilde{v}^2}/\overline{v^2})_m(\%)$	54.3	30.3	20.0	25.7	42.0	27.2	78.7	75.7	69.0
$(\overline{\tilde{\theta}^2}/\overline{\theta^2})_m(\%)$	13.5	6.8	4.0	13.0	15.9	9.2	50.1	39.6	44.9
$(\overline{\tilde{u}\tilde{v}}/\overline{uv})_m(\%)$	60.4	19.2	17.5	26.9	44.2	28.7	67.4	65.4	103.4
$(\overline{\tilde{u}\tilde{\theta}}/\overline{u\theta})_m(\%)$	91.7	23.9	10.1	17.7	72.6	28.0	93.1	112.3	131.7
$(\overline{\tilde{v}\tilde{\theta}}/\overline{v\theta})_m(\%)$	57.5	25.6	14.2	28.2	42.7	25.4	71.2	49.7	88.1

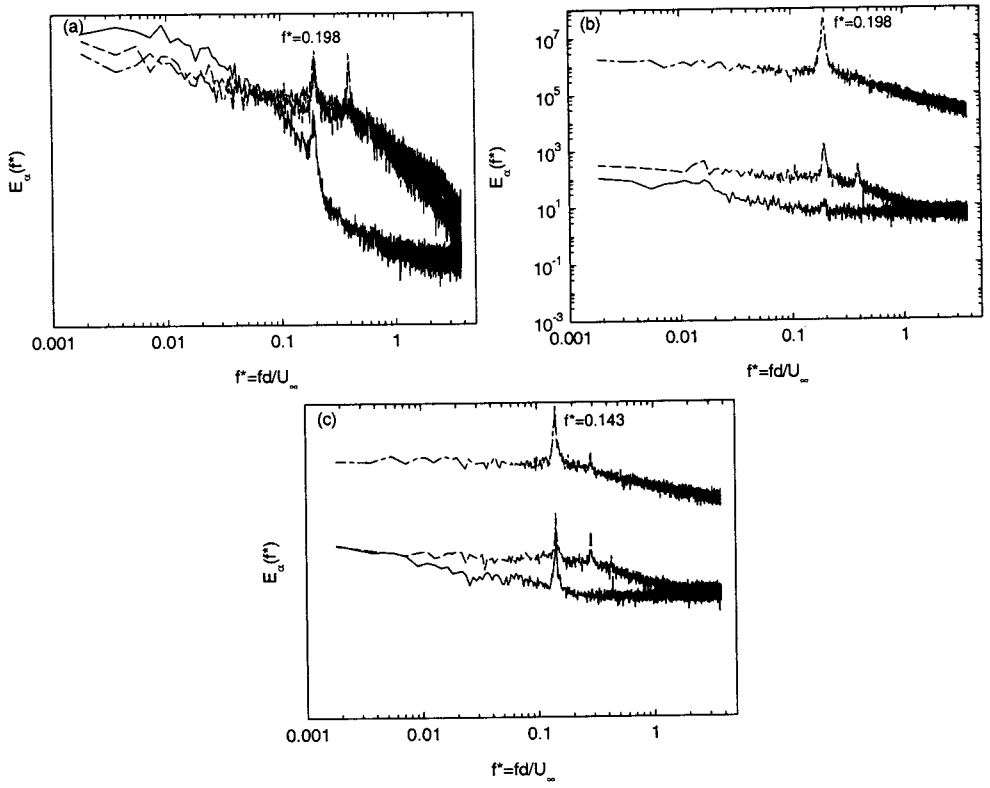

Figure 1. Power spectra of u, v and θ at half the wake half-width for x/d=10. (a) L/d=1.3; (b): 2.5; (c): 4. – – –, α=u; — – — –, v; ——, θ.

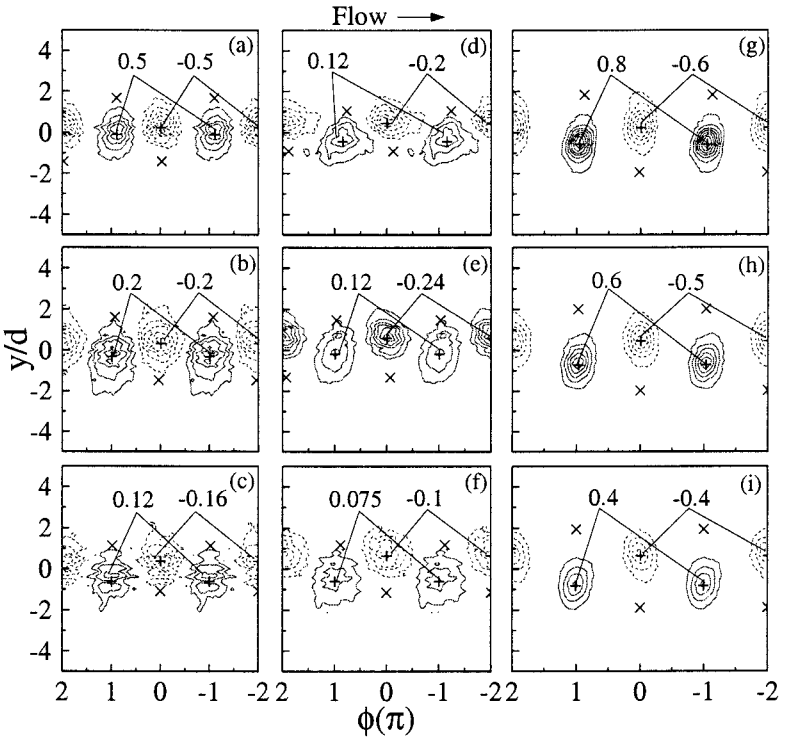

Figure 2. Phase-averaged vorticity contours $\tilde{\omega}^*$. (a-c) L/d = 1.3: (a) x/d = 10, contour interval = 0.1; (b) 20, 0.04; (c) 30, 0.04. (d-f) L/d = 2.5: (d) 10, 0.04; (e) 20, 0.04; (f) 30, 0.025. (g-i) L/d = 4.0: (g) 10, 0.1; (h) 20, 0.1; (i) 30, 0.1.

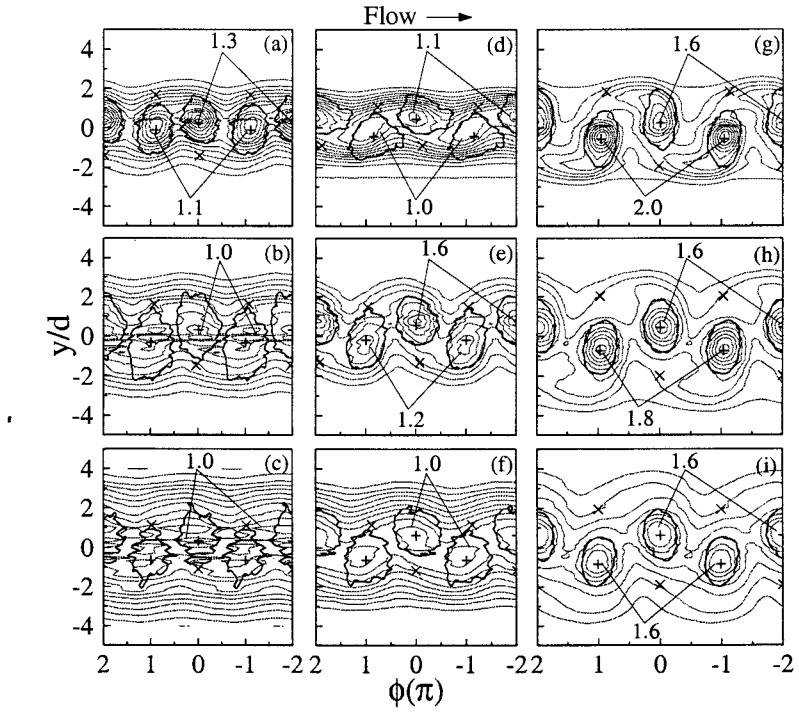

Figure 3. Phase-averaged temperature contours $\overline{\Theta}^* + \tilde{\theta}^*$. (a-c) L/d = 1.3: (a) x/d = 10, contour interval = 0.1; (b) 20, 0.1; (c) 30, 0.1. (d-f) L/d = 2.5: (d) 10, 0.1; (e) 20, 0.2; (f) 30, 0.1. (g-i) L/d = 4.0: (g) 10, 0.2; (h) 20, 0.2; (i) 30, 0.2. The thicker solid line denotes the outermost vorticity contours.

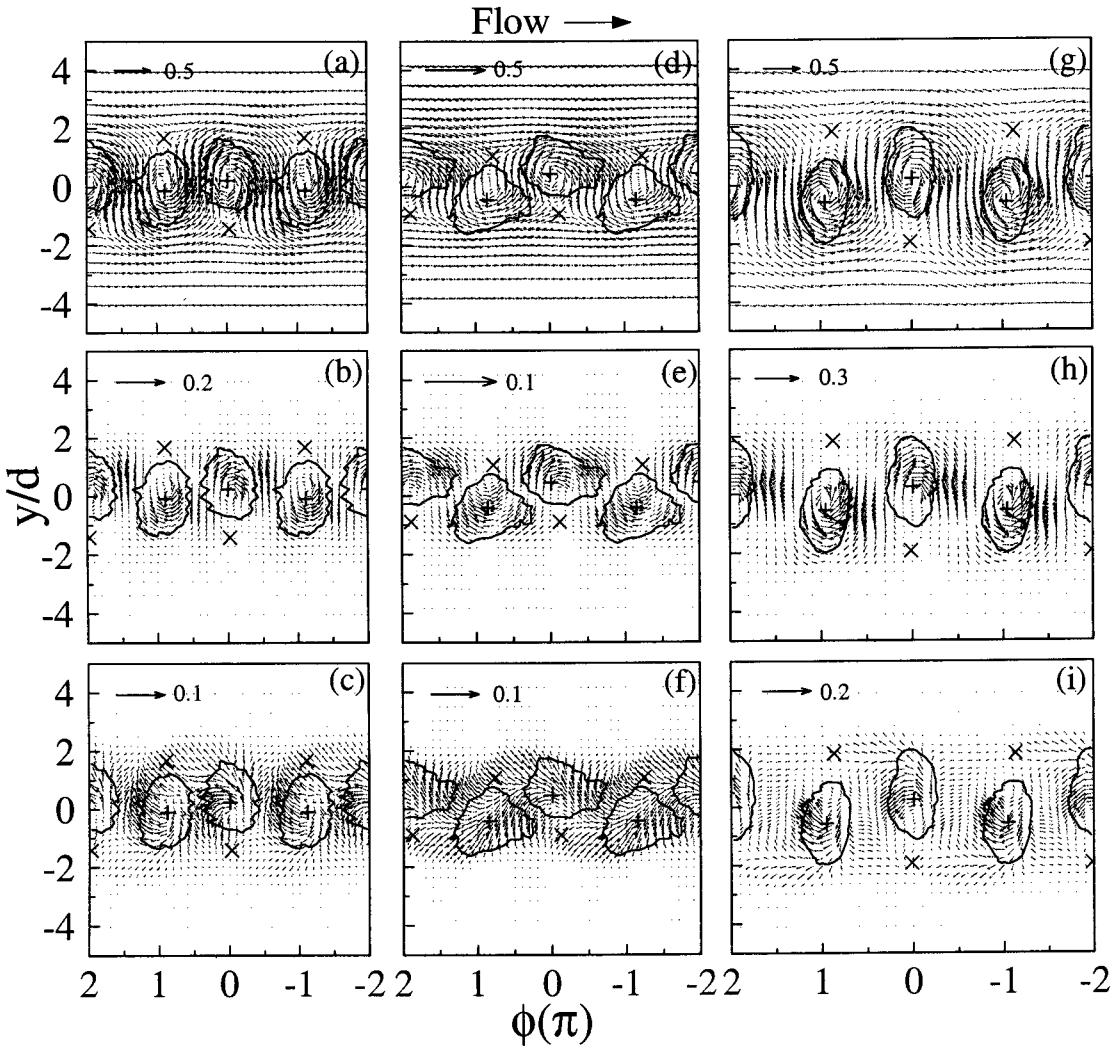

Figure 4. Phase-averaged coherent velocity vectors $\tilde{V}^*$ moving at U_c and coherent heat flux vectors $\tilde{q}^*$ and incoherent heat flux vectors $\tilde{q}_r^*$ at $x/d = 10$. $\tilde{V}^*$: (a) $L/d = 1.3$ (d) 2.5 (g) 4.0. $\tilde{q}^*$: (b) $L/d = 1.3$ (e) 2.5 (h) 4.0. $\tilde{q}_r^*$: (c) $L/d = 1.3$ (f) 2.5 (i) 4.0. The thicker solid lines denote the outermost vorticity contours.